Pergamon

Int. J. Heat Mass Transfer. Vol. 37, No. 3, pp. 425–436, 1994

0017–9310/94 $6.00 + 0.00

Evaporative heat transfer and enhancement performance of rib-roughened tube annuli with refrigerant 114

MAO-YU WEN and SHOU-SHING HSIEH†

Department of Mechanical Engineering, National Sun Yat-Sen University, Kaohsiung, Taiwan 80424, R.O.C.

(*Received* 25 *August* 1992 *and in final form* 27 *July* 1993)

Abstract—Heat transfer and pressure drop measurements were performed on three rib type roughened tube annuli (4.67–6.93 mm D_h, 9–16 ribs, rib pitch 19.7–39.4 mm, rib height 4 mm, rib width 15 mm, rib angle 30–60°) with two-phase flow of refrigerant R-114 under evaporating condition. The data were compared with the performance of a smooth tube annulus (6.5 mm D_h). Based on the same heat transfer area (≈ 4.24 cm^2) of the test section, changes in mass velocity range (63.55–129.86 kg m^{-2} s^{-1}) and heat flux level ($2.01–2.95 \times 10^4$ W m^{-2}) on heat transfer coefficient and pressure drop with the varied quality were conducted and the influences were studied. Enhancement performance ratios are also presented and discussed. Moreover, flow boiling experiments with rib type roughened surfaces using R-114 through flow visualization were explored to broaden our fundamental understanding of the boiling heat transfer mechanism.

INTRODUCTION

RECENT technological implications have given rise to increased interest in enhancement of the in-tube evaporation used in many air conditioning and refrigeration systems. Various techniques have been used to improve heat transfer characteristics of in-tube flow. Several experimental studies have investigated evaporation of standard refrigerants inside internally finned tubes [1]. Lavin and Young [2] used Refrigerant 12 (R-12) and Refrigerant 22 (R-22) to study horizontal and vertical flow through electrically heated tubes with fins about 2.54 mm high and spiral angles of 0.0–7.08°. Spiral tubes had slightly better performance. Kubanek and Miletti [3] conducted three finned tube tests with R-22 heated with water at high pressure. Ito and Kimura [4] studied heat transfer and pressure drop of R-22 in internally finned horizontal tubes. The fins were triangular. A later study by Kimura and Ito [5] used the same apparatus to study heat transfer in 4.75 mm-i.d. tubes at low flow rates. The best heat transfer performance in annular flow was obtained with tubes having 15° spiral fins. Tatsumi *et al.* [6] investigated evaporation of R-22 in two 8.72-mm-i.d. tubes. Both tubes had numerous low fins with a 7.0° spiral. These are referred to as microfin tubes. It was found that heat transfer coefficients were higher with larger fin heights and that the larger coefficients were obtained when the spiral angle was around 10°. Tojo *et al.* [7] tested evaporation heat transfer and pressure drop in 8.82-mm-i.d., microfin tubes with R-22. Tojo reported the highest heat transfer coefficients from the tube with sawtooth-shaped fins having a 25° spiral. In addition, several studies have reported data for refrigerants evaporating inside tubes with twisted-tape inserts [8–10].

Other surfaces, for instance, rib type surfaces which provide for more stable sites are potentially more attractive as far as the boiling heat transfer is concerned. While the mouth of the cavity between two consecutive ribs determines the superheat required to nucleate, the internal shape and volume together with the wetting characteristics of the cavity walls determine the stability of the nucleating cavity. It has been shown [11] that re-entrant cavities of the shape are very stable and will continue to nucleate when conical cavities have been snuffed out. The concept of this type of roughened surface is known in France as the 'Vapotron' [12] and is used to cool electronic power tubes dissipating heavy heat loads.

Although many past studies have examined in-tube evaporative heat transfer enhancement and the associated pressure drop with internally finned tubes. In-tube evaporations with rib type surface attachments using R-114 as refrigerant have not been conducted. In addition, the fundamental phenomenon of nucleate boiling from a heated wall subject to a rib type roughness surface is as yet not well understood. In this study, flow boiling tests were conducted in horizontal tube annuli with surface attachments. Attention was given to the heat transfer enhancement as well as pressure drop measurement and to the influences of nucleate boiling on the test tubes. Different cases in terms of varied rib angles and pitches were tested.

EXPERIMENTAL APPARATUS AND PROCEDURE

The experimental apparatus consisted of a horizontal test section with R-114 flowing at 2–3 times

† Author to whom correspondence should be addressed.

NOMENCLATURE

A	heat transfer area, $2\pi r_e L$ [cm^2]	Greek symbol	
D_h	hydraulic diameter of annulus, $2(r_o - r_e)$ [mm]	θ	rib angle.
G	mass velocity [kg m^{-2} s^{-1}]		
H	rib height [mm]	Subscripts	
h	wall heat transfer coefficient [W m^{-2} K^{-1}]	a	augmented tube
		avg	average
k	thermal conductivity [W m^{-1} K^{-1}]	bot	bottom outside of tube wall
L	length of test tube [mm]	e	equivalent
P	pressure [kg cm^{-2}]	mid	middle outside of tube wall
p	rib pitch [mm]	in	inlet
r_e	radius of equivalence circular tube defined in equation (2) [mm]	i	inside diameter
		o	outside diameter
Q	heat transfer rate [W]	s	smooth tube
q	wall heat flux [W m^{-2}]	sat	saturated
T	temperature [°C]	sub	liquid subcooling at test section inlet
X	quality (flowing mass fraction of vapor)	TP	two-phase
V	voltage	top	top outside of tube wall
w	rib width [mm].	w	tube wall.

atmospheric pressure in a closed loop as shown in Fig. 1. This flow loop consisted of a preevaporator, preheater, dryer, test section, receiver, condenser, pump and after-pump. The test section is made of a conventional double-pipe heat exchanger (see Fig. 1 for details). The inside diameter of the outer tube (D_o) is 45 mm with outside tube diameter (d_2) of the isoflux heated inner tube of 19 mm. The outside tube was prepared by Plexiglas pipe (45 mm i.d., 51 mm o.d.) to facilitate the flow visualization. A series of copper ribs (the size and geometry are given in Table 1) on a copper ($k = 111$ W m^{-1} K^{-1}) tube (350 mm × 19.0 mm × 13.9 mm). The electric wire was packed into the copper tube. Heating was provided by conducting dc through the electric wire. A two-walled structure (MgO + quartz) was sandwiched between the copper tube and the electric wire as an electrical shield (see Fig. 1 for details). A series of bypasses and regulators controlled the R-114 flow rate and pressure in the test section.

The preevaporator preheated R-114 to a saturation condition (within ±0.3°C). As R-114 flowed through the test section, it was uniformly heated by dc power passing through the wall of the tube. The dc power was provided by a 100 V, 550 A capacity dc rectifier. Power to the test section was controlled with a remote

Table 1. The size of test tubes and working fluid (R-114) properties

Test tube	Tube (No.)	d_1 (mm)	d_2 (mm)	D_h (mm)	Number of rib elements	p (mm)	w (mm)	H (mm)	θ	A (cm^2)
Rib	1	27	19	6.93	9	39.4	15	4	30°	4.22
Rib	2	27	19	5.76	13	26.3	15	4	45°	4.26
Rib	3	27	19	4.67	16	19.7	15	4	60°	4.21
Smooth	4	—	—	6.50	—	—	—	—	—	4.24

Properties	Unit	Value
Molecular weight	kg kmol^{-1}	170.92
Pressure	kg cm^{-2}	2.55
Saturated temperature	°C	30.0
Liquid density	kg m^{-3}	1440.8
Vapor density	kg m^{-3}	13.38
Liquid specific heat	kJ kg^{-1} K^{-1}	1.11
Heat of evaporation	kcal kg^{-1} K^{-1}	30.17
Liquid thermal conductivity	m W m^{-1} K^{-1}	64.0
Liquid viscosity	μPa s	334.8
Vapor viscosity	μPa s	11.82
Surface tension	N m^{-1}	0.01
Prandtl number	—	5.38

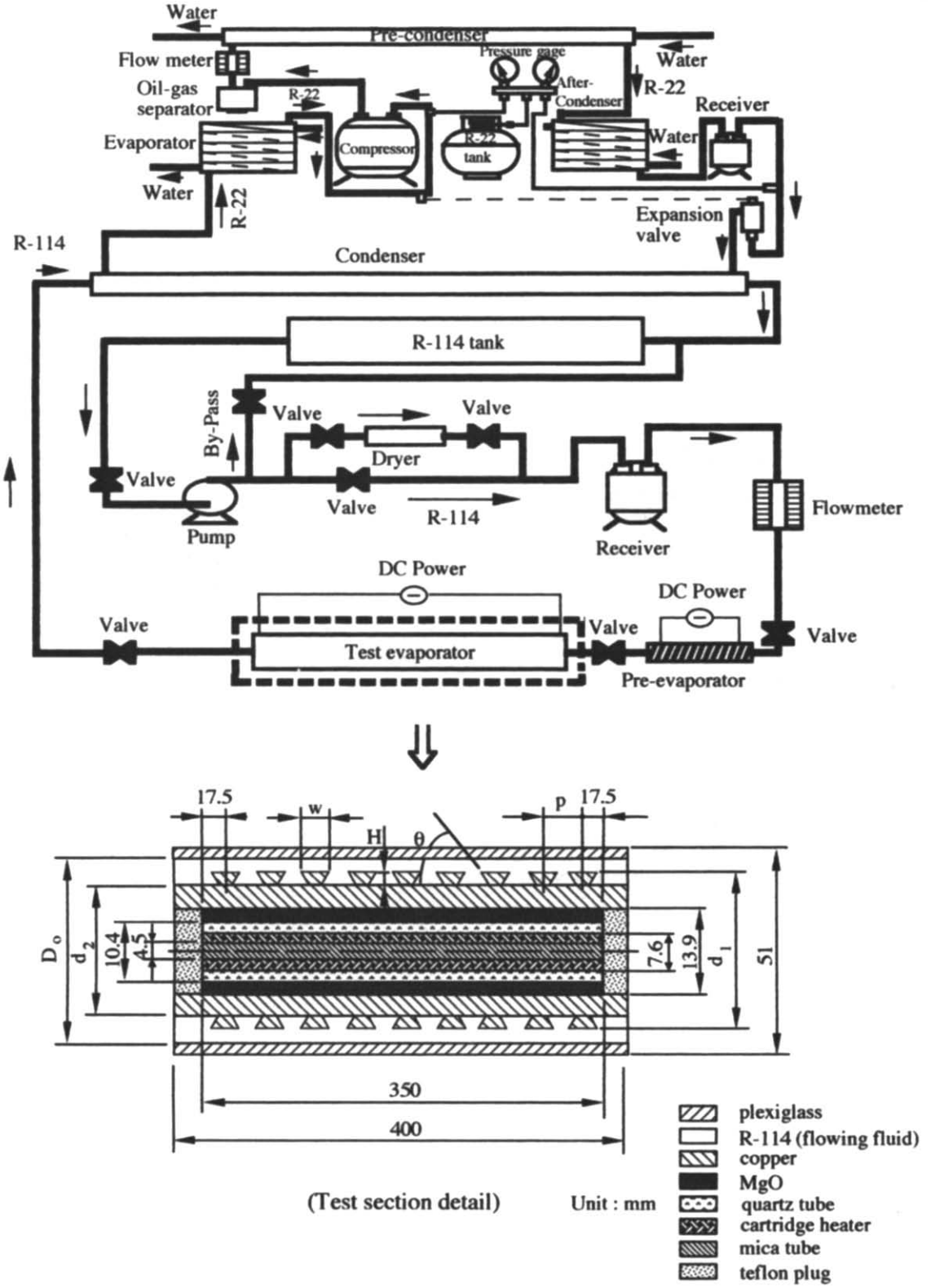

FIG. 1. Schematic of experimental apparatus.

Table 2. Ranges of experiments and measurement uncertainties

Parameters	Range	Uncertainty
Mass velocity, G	63.55, 93.74, 129.86 ($kg\,m^{-2}\,s^{-1}$)	±3.1%
Heat flux supplied to test section, $\dot{q}$	2.01, 2.43, 2.95×10^4 ($W\,m^{-2}$)	±4.3%
Local quality in the test section, x	0.015–0.8	±5.7%
Average pressure over the test section, $\bar{p}$	2.53–2.83 ($kg\,cm^{-2}$)	±4.5%
Wall temperature, T_w	32–45 (°C)	±1.0%
Wall heat transfer coefficient, h	$4.1-8.9\times10^3$ ($W\,m^{-2}\,°K^{-1}$)	±7.1%
Enhancement performance ratio, $(h_a/h_s)/(\Delta p_a/\Delta p_s)$	0.92–1.54	±9.4%

control box. After exiting the test section, the R-114 passed to the R-22 cooled condenser where it was condensed and subcooled prior to being returned to the pump to complete the circuit.

Figure 2 shows the locations of temperature and pressure measurements of the test section. Bulk fluid temperatures at the inlet and exit of the test section were measured with 40 gage copper–constantan thermocouples located at midstream. The inlet and outlet pressures were measured with a calibrated pressure gage, respectively. Intermediate bulk fluid temperatures were measured at a certain distance (50 mm each) along downstream location (see Fig. 2 for details). The R-114 flow rate was measured by a rotameter (Flowmeter Mold HFM201, SERIAL 811) located between the condenser and preevaporator. Thermocouples measured wall temperature at 13 locations along the test section (see Fig. 2 for details). These thermocouples were carefully inserted into the outside wall of the inner tube. A detailed cross-sectional view of the thermocouples setup designed for more accurate temperature measurements was also shown in Fig. 2. Based on calibration of the entire temperature measurement system including thermocouple and digital voltmeter, the error associated with the temperature data was estimated to be ±0.3°C.

The dimensions of the tubes tested as well as R-114 properties are listed in Table 1. The parameter D_h is defined as:

$$D_h = 2(r_o - r_c) \tag{1}$$

which corresponds to a bare inner tube of radius r_c. A bare tube of radius r_c provides the same surface as the ribbed tube, i.e.

$$r_c = \left[2\left(r_i + \frac{H}{2}\right)\frac{H}{\sin\theta} + (r_i + H)w + r_i\left((p-w) + \frac{2H}{\tan\theta}\right)\right]\Big/ p. \tag{2}$$

Also shown in Table 1 is the tube numbering system (i.e. Tubes 1–4) which is used throughout this paper to identify each tube. Before each test, the test tubes were cleaned with acetone. The test fluid flow loop was pressure tested for leaks. The leaks were detected by using a soapy water solution. A test was started by first boiling the liquid for 2–3 h to drive away air content in the system. Table 2 shows the ranges of variables over which the experiments were conducted and the associated measurement uncertainties.

DATA REDUCTION

A number of roughened tubes with different rib pitches and rib angles and smooth tubes were tested by R-114 at an average pressure of 2.68 $kg\,cm^{-2}$. Each tube was tested at an inlet pressure of approximately 2.41 $kg\,cm^{-2}$ and an inlet temperature of approximately 30°C.

For each test run, six axial heat transfer coefficients were calculated on the basis of bulk fluid saturation temperature, tube heat flux and tube inside wall temperature. Three thermocouples were mounted just downstream of each pressure tap; hence, the readings were averaged

$$T_{avg} = (T_{top} + T_{mid} + T_{bot})/3. \tag{3}$$

Wall temperatures at all other locations were based on the single measurement, T_{mid}. Circumferential variations in wall temperature were normally negligible in the forced convection vaporization region, and somewhat larger (but still less than 0.2°C) in the nucleate boiling region. The local heat transfer coefficient at each axial location was then calculated as follows:

$$h = Q/A(\bar{T}_w - T_{sat}). \tag{4}$$

When heat transfer coefficients were calculated for roughened tubes, the area used in equation (4) was the surface area of $\pi D_h L$. Mass flux was also based on the cross-sectional area calculated from the equivalent diameter D_h. Qualities at each axial location were calculated from inlet conditions and energy balances along the tube length. The uncertainties in the heat transfer coefficient and quality calculations were listed in Table 2. The pressure drop data were measured over a length of 0.05 m for the test section (0.35 m). The effect of natural convection in the experiments reported herein can be considered to be negligible due to the parameter (Grashof number/(Reynolds number)^2) being much less than unity even at the lowest mass velocity.

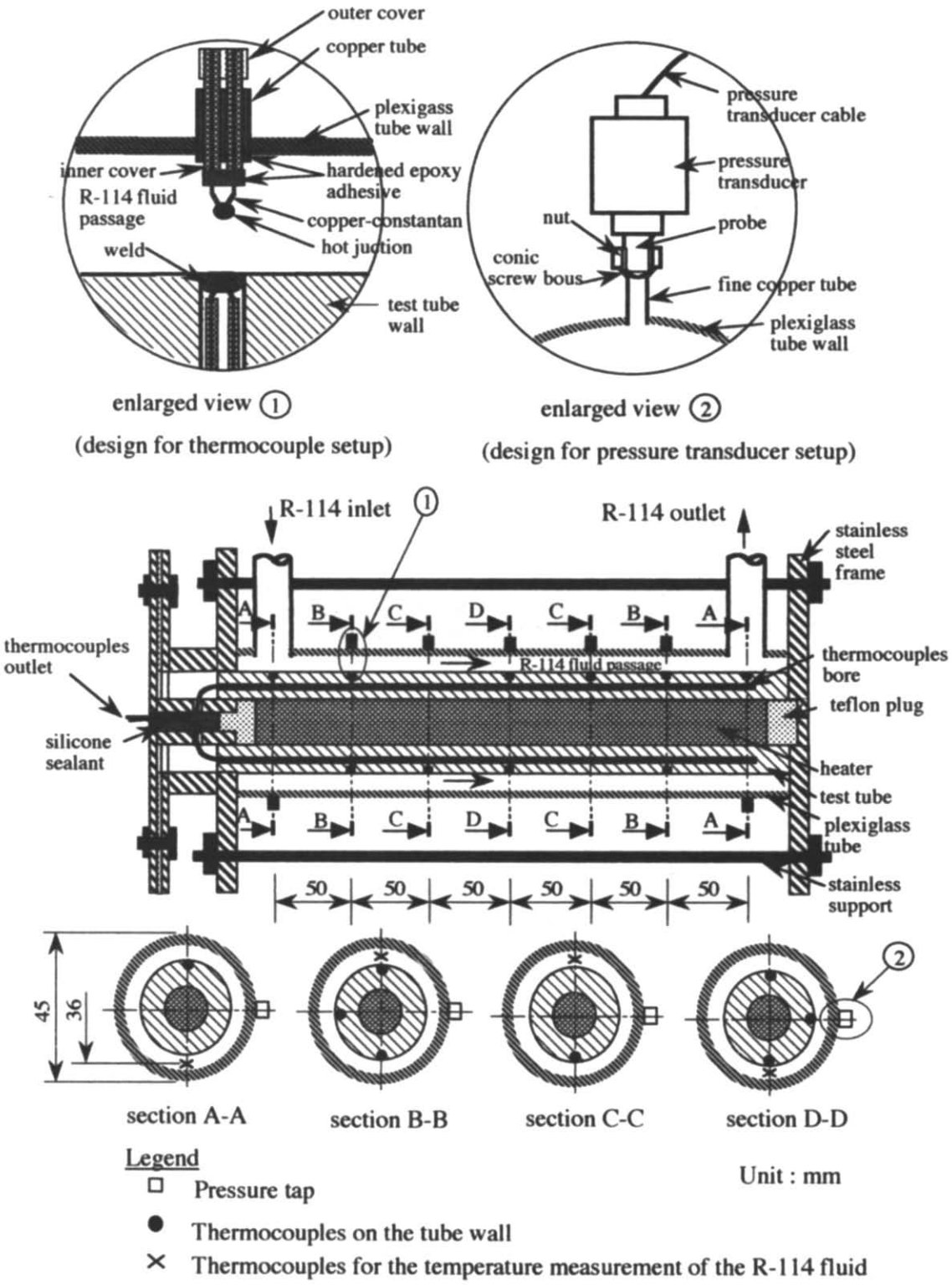

FIG. 2. Locations of temperature/pressure measurements for the test evaporator (not to scale).

RESULTS AND DISCUSSION

Several single phase heated tube tests were performed for R-114 prior to nucleate flow boiling tests and the results were compared to the well-known Dittus–Boelter equation [13]. It was found that they were in good agreement within an average deviation of ±25%. For each of these tests, an energy balance analysis was made for the entire loop. The energy gained by the R-114 across the entire test section was compared to the sum of the power input and heat gain from the surroundings. For all these tests, the analysis found that the energy balance was satisfied within 9.3%.

The system was judged to have reached a steady-state condition when the temperatures, pressures and mass flux rates of R-114 fluid remained unchanged for about 2 h. A series of tests were carried out for refrigerant R-114. The ranges of heat flux and mass velocity considered for this study were 20.1, 24.3, and 29.5 kW m^{-2} and 63.55, 93.74, and 129.86 kg m^{-2} s^{-1}. In order to avoid physical burnout of the test section, qualities at the outlet of the test section were adjusted not to exceed 0.8. Figure 3 shows single liquid forced convection and saturated nucleate boiling heat transfer data at two mass velocities (63.55 and 129.86 kg m^{-2} s^{-1}) at a measurement plane pressure of 2.55 (kg cm^{-2}) (this corresponded to R-114 saturated pressure) and a liquid temperature at the test section inlet of 30°C. The data shown pertain to increasing-heat flux mode. In Fig. 3 the wall heat flux has been plotted vs the wall superheat. A partial nucleate boiling in which the heat transfer mechanism may be sensitive to variations in mass velocity was noted in Tubes 1, 2 and 3. A significant enhancement of nucleate boiling was observed with these rib type roughened tubes, regardless of whether there is an increase in the mass velocity, as compared to those of smooth tubes.

This is because the present roughened surface leaves

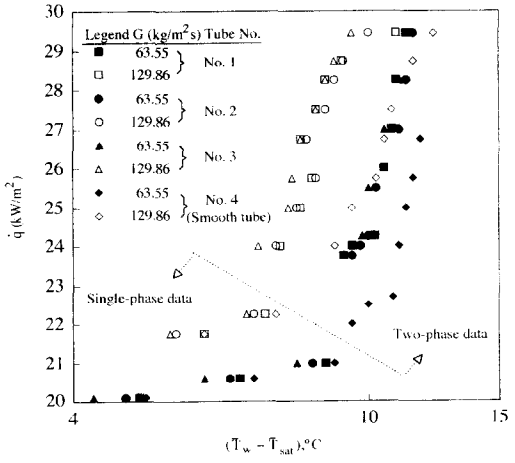

FIG. 3. Flow boiling curves at two mass velocities for four test tubes.

a surface structure which comprises of a series of tunnels connected to the R-114 by regularly spaced pores. The configuration provides regularly spaced re-entrant cavities and greatly enhanced nucleation properties. Consequently, it triggers the onset of nucleate boiling earlier than it usually does in smooth tubes. Furthermore, Tubes 1, 2 and 3 at $G = 129.86$ kg m^{-2} s^{-1}, seem to have the same heat transfer rates. This behavior also happened at $G = 63.55$ kg m^{-2} s^{-1}.

It is interesting to note that the independence of the heat transfer process in the partial nucleate boiling on the mass velocity no longer exists. This may be attributed to the contribution of the roughened surfaces on the part of forced convection in partial nucleate boiling region. The data in Fig. 3 show that the enhancement was more pronounced in the higher mass velocity where nucleate boiling on the roughened surfaces was not fully established and the enhancement due to bubble motion became relatively more important. It was observed that they were generated at lower frequency from the vicinity of roughened surface than that with $G = 63.55$ kg m^{-2} s^{-1}. As a result, the data demonstrate a bigger improvement in heat transfer rate. The bigger improvement is due to many bubbles moving along the heated surface, and much thermal layer removal and film evaporation. In summary, the result from Fig. 3 revealed that nucleate boiling can be enhanced by applying the present rib roughened surfaces attachment to a horizontal tube annulus, owing to the favorable thermal environment characterized by a small gradient liquid temperature profile within the restricted regions between the rib and the heated surface. Nucleate boiling is enhanced in terms of a lower wall superheat required for incipient boiling and more and stable bubbles generated than from a smooth tube.

The definition of wall heat transfer coefficient given by equation (4) pertains to both single phase liquid flow and boiling flow in this work. Figure 4(a) depicts the comparison of the experimental heat transfer coefficient data with the correlation by Shah [14] for the cases shown. The Shah correlation reduces to the Dittus–Boelter correlation in the event of single phase liquid flow. Most of the data were within ±20% of the predicted values. A series of repeatability tests indicated a maximum variation about ±7.1% in the heat transfer coefficients. A comparison of experimental pressure drop data with the Lockhart and Martinelli [15] correlation is shown in Fig. 4(b). No correlation was made for the acceleration part because it is so small compared to its counterpart. The data points are within ±30% of the predicted values with the maximum deviation occurring at the low mass velocity. The large deviation from the correlation is not unusual for two-phase flow.

The effect of roughened surfaces on the heat transfer coefficient is shown in Fig. 5 for two different mass velocities at a given heat flux. In general, an increase in mass velocity increases the heat transfer coefficients for all the qualities plotted. For Tubes 1, 2 and 3, at

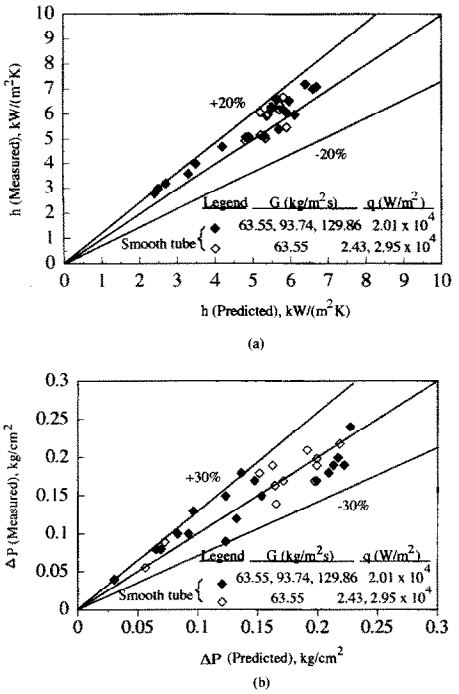

FIG. 4. Comparisons between measured and (a) predicted evaporation heat transfer coefficients (Shah correlation [14]), (b) predicted pressure drops (Lockart–Martinelli correlation [15]).

$G = 129.86$ kg m^{-2} s^{-1}, the heat transfer coefficients were observed to be independent of the quality. In contrast, an increase in the quality decreases the heat transfer coefficient at $G = 63.55$ kg m^{-2} s^{-1}. This is perhaps because, at higher quality for low mass velocity ($G = 63.55$ kg m^{-2} s^{-1}), a flow pattern transition from bubbly or slug to annular flow instead results in

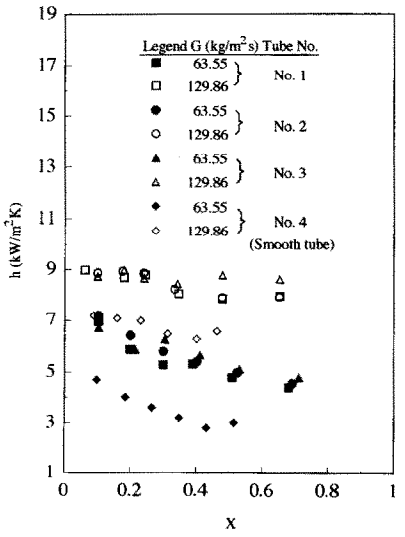

FIG. 5. Flow boiling heat transfer coefficients varied with quality at heat flux $\dot{q} = 20.1$ kW m^{-2} for various mass velocities.

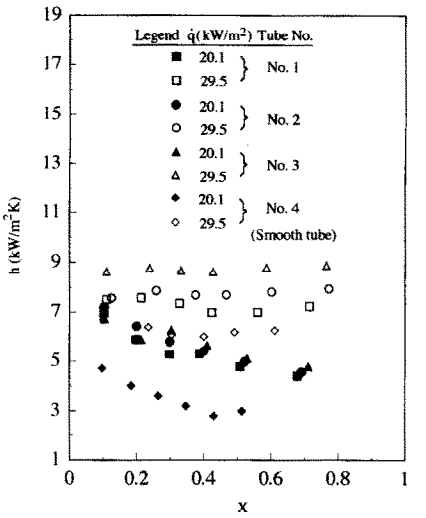

FIG. 6. Flow boiling heat transfer coefficients varied with quality at mass velocity $G = 63.55$ kg m^{-2} s^{-1} for various heat flux.

the forced convective region which is chracterized by this annular liquid film with convection and conduction heat transfer at the liquid–vapor interface. Consequently, this results in a heat transfer coefficient decrease. In addition, in this partial nucleate boiling region, both the forced convection and nucleate boiling mechanisms are significant. The gradual suppression of the latter leads to a reduction of the heat transfer coefficients with increasing quality at low mass velocity, which was also observed in ref. [16]. Figure 6 shows the effect of heat flux on the heat transfer coefficient for all the tubes tested. The heat flux was varied by 50%. An increase in heat flux generally increases the heat transfer coefficients. Rough surface resulting in a heat transfer enhancement was significantly observed at higher heat flux ($\dot{q} = 2.95 \times 10^4$ W m^{-2}). However, the effect was not clearly noted at lower heat flux ($\dot{q} = 2.01 \times 10^4$ W m^{-2}). It is known that the transition point from the partial boiling to the two-phase convective region is shown to be a function of heat flux such that it moves to a higher quality as heat flux increases for a given mass velocity. Beyond this transition quality, however, the line for the various heat fluxes merge into a single line indicating that nucleate boiling is suppressed. According to the foregoing statements, it strongly suggests that the onset of transition quality was delayed to occur for the present study. Furthermore, for both Figs. 5 and 6, it was shown that the heat transfer coefficient was almost independent of quality for the roughened tubes (Tubes 1, 2, and 3) at higher mass velocity and heat flux.

Of special interest for studies of heat transfer augmentation is the question of how much the heat transfer coefficient is increased relative to an equivalent smooth tube at the same condition for the present study. Local enhancement factors (h_a/h_s) were calculated by forming ratios of experimentally measured

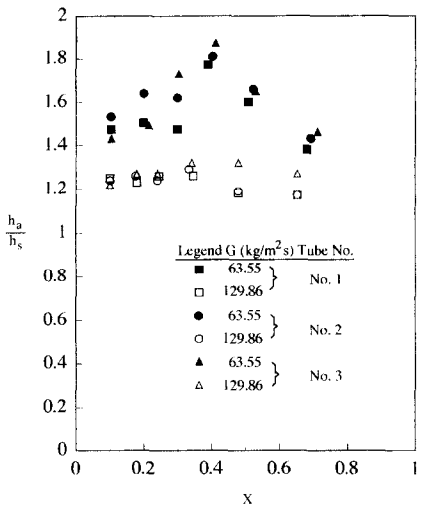

FIG. 7. Heat transfer enhancement factors varied with quality at heat flux $\dot{q} = 20.1$ kW m^{-2} for various mass velocities.

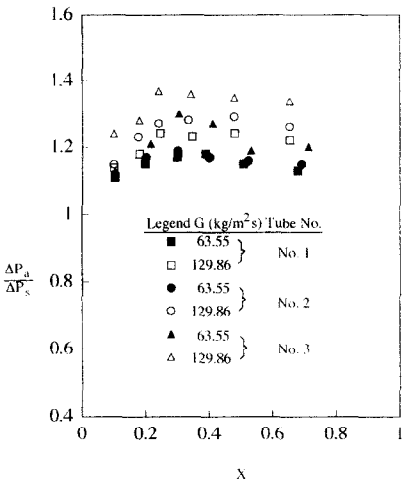

FIG. 9. Pressure gradient ratios varied with quality at heat flux $\dot{q} = 20.1$ kW m^{-2} for various mass velocities.

heat transfer coefficients for the roughened tube and a smooth tube of the same heat transfer area. As shown in Fig. 7, the enhancement factors at $\dot{q} = 2.01 \times 10^4$ W m^{-2} for the three roughened tubes are about the same (≈ 1.25) at higher mass velocities. In contrast, the distribution of the local enhancement factor exhibits a different trend. It shows a steady increase starting from $X = 0.1$ and, after reaching a peak at $X = 0.4$, then gradually decreases to a local minimum value about 1.4 at $X = 0.7$. It is somewhat surprising that the enhancement factors are similar for both the magnitude and trend for three different roughened tubes at lower mass velocity. Figure 8 exhibits the same behavior as Fig. 7 at a given mass velocity $G = 63.55$ kg m^{-2} s^{-1} with two different heat flux levels. However, it suggests that the lower heat flux has a higher enhancement factor. This is perhaps because the forced convection region at higher heat flux was more effective than at lower heat flux level. This may result in a thicker liquid film and, therefore, lower values in heat transfer coefficient. This speculation is supported by the work of Reidy [17].

Figures 9 and 10 indicate the pressure gradient ratios, $\Delta p_a/\Delta p_s$ for all the tubes at $\dot{q} = 2.01 \times 10^4$ W m^{-2} and $G = 63.55$ kg m^{-2} s^{-1}, respectively. The pressure gradient ratios stand for the increases in pressure drop for roughened tubes relative to the smooth tubes expressed as a pressure drop enhancement factor ranged from 1.1 to 1.38. As shown in Fig. 9, the pressure gradient ratio is higher as the number of ribs and the heat flux levels are increased. The pressure drop increases over the corresponding smooth tube due to the reduced (by $\approx 5\%$) cross-sectional flow area. In addition, the distinction in magnitude of the

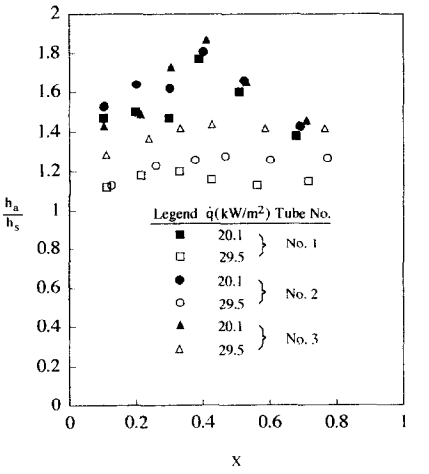

FIG. 8. Heat transfer enhancement factors varied with quality at mass velocity $G = 63.55$ kg m^{-2} s^{-1} for various heat flux.

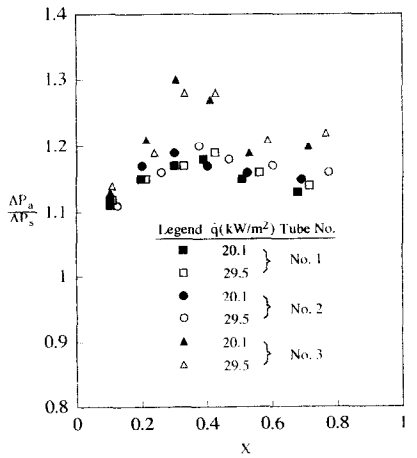

FIG. 10. Pressure gradient ratios varied with quality at mass velocity $G = 63.55$ kg m^{-2} s^{-1} for various heat flux.

pressure gradient ratio is clearly noted at higher heat flux. This is mainly because the acceleration effect was much higher. However, this phenomenon was not found at lower heat flux except in the range of $X \approx 0.2$–0.4 for Tube 3. In general, the pressure drop increased with increases in the mass velocity at a given heat flux $\dot{q} = 2.01 \times 10^4$ W m^{-2}. But, this behavior is not preserved for different heat flux levels at a given mass velocity as shown in Fig. 10. For both Figs. 9 and 10, the pressure drop was not a strong function of quality. As stated earlier, Tube 3 had the highest pressure drop. Furthermore, the pressure gradient ratio for Tube 3 in Fig. 9 is considerably higher varying from 1.25 at $X = 0.1$ to 1.35 at $X = 0.65$.

The effects of heat transfer and pressure drop can be combined into one parameter called the enhancement ratio $((h_a/h_s)/(\Delta p_a/\Delta p_s))$ which is shown in Figs. 11 and 12, respectively, at $\dot{q} = 2.01 \times 10^4$ W m^{-2} and $G = 63.55$ kg m^{-2} s^{-1}. From this viewpoint of maximizing heat transfer while minimizing pressure drop, higher values are most desirable. For most tubes tested, the pressure gradient ratio was observed to be lower than the heat transfer enhancement factor which results in an enhancement performance ratio higher than 1. These are the cases shown in Figs. 11 and 12. Because of the larger pressure gradient ratio for Tube 3, the enhancement performance ratio for Tube 2 is greater over most of the quality range shown in both Figs. 11 and 12. Specifically, in Figs. 11 and 12, at $X \approx 0.2$ Tube 2 has an enhancement performance ratio of 1.4 while Tube 3 has a value 1.24. In general, additionally, it was found that enhancement performance ratio was not a strong function of quality at the higher mass velocity and heat flux but it is strongly dependent on quality at the lower mass velocity and heat flux.

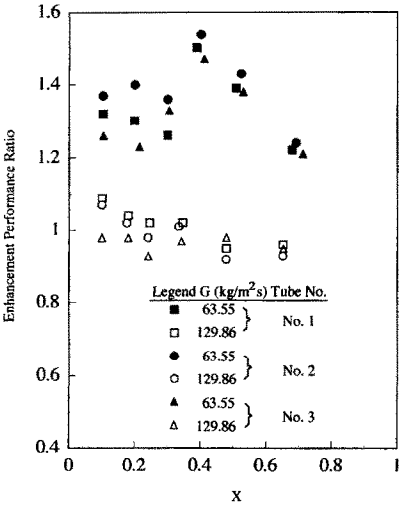

FIG. 11. Enhancement performance ratios varied with quality at heat flux $\dot{q} = 20.1$ kW m^{-2} for various mass velocities.

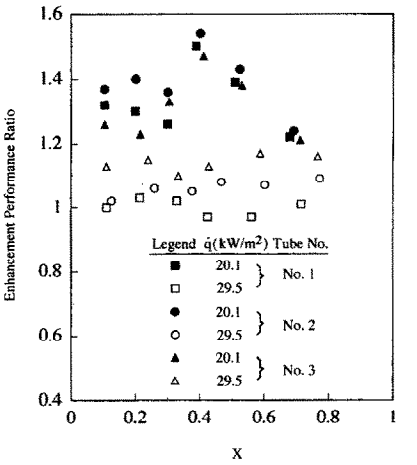

FIG. 12. Enhancement performance ratios varied with quality at mass velocity $G = 63.55$ kg m^{-2} s^{-1} for various heat flux.

Table 3 documents the present enhancement performance ratio vs varied quality under different working conditions. Also listed in Table 3 is the previous work by Reid *et al.* [18] in which fin tube and helical tape with R-113 as a working fluid were used. The present results are superior to those of ref. [18] in most cases.

Figure 13 shows typical photographs made by flow visualization of the present flow boiling in Tube 3 and smooth tubes at different mass velocities and heat flux level. Starting from Figs. 13(e) and (f), one may find that bubbles rise from isolated nucleation site ($G = 63.55$ kg m^{-2} s^{-1} and $\dot{q} = 2.01 \times 10^4$ W m^{-2}). As the heat flux ($\dot{q} = 2.95 \times 10^4$ W m^{-2}) and mass velocity ($G = 129.86$ kg m^{-2} s^{-1}) increase, more and more sites are activated. On the other hand, in Figs. 13(a)–(d) for roughened tube annuli, the active sites become very numerous, the bubbles start to merge into one another, and an entirely different kind of vapor escape path seems to come into play, especially for the extreme case ($G = 129.86$ kg m^{-2} s^{-1} and $\dot{q} = 2.95 \times 10^4$ W m^{-2}). Boiling takes place in the two consecutive ribs. It is known that the outer space temperature of the ribs varies with location according to the modes of heat transfer taking place (e.g. stable nucleate boiling and transition boiling). Vapor formed at the surface merges immediately into jets which are carried away in the downstream due to the present flow boiling. This phenomenon was found in Figs. 13(a) (d) and is most distinct in Fig. 13(d). It is apparent for Fig. 13 that the number of active nucleation sites generating bubbles would be strongly influenced by heat flux and mass velocity as well as the present surface condition. It is found that the present surface (roughened tubes) condition can generate more smaller and smaller vapor pockets which will be triggered into active bubble growth to reduce the wall superheat $(\bar{T}_w - T_{sat})$ for incipient boiling compared to those for smooth tubes. This also verifies the previous findings in Fig. 3.

Table 3. Comparison with Reid *et al.* [18] for enhancement performance ratios

Investigators	Geometry of the test tube: Augmentation method	Material	Tube No.	Fluid	Conditions: P_{in} (kg cm^{-2})	ΔT_{sub} (°C)	q (W m^{-2})	G (kg m^{-2} s^{-1})	Enhancement performance ratio† $X=0.1$	$X=0.2$	$X=0.3$	$X=0.4$	$X=0.5$	$X=0.6$	Average
Present study	Consecutive ribs	Cu	No. 1	R-114	2.01	0	2.01×10^4	63.55	1.33	1.30	1.26	1.45	1.40	1.32	1.34
								129.86	1.09	1.04	1.02	1.00	0.95	0.95	1.01
					2.01	0	2.01×10^4	63.55	1.32	1.30	1.26	1.45	1.39	1.30	1.33
							2.95×10^4		1.00	1.03	1.02	0.98	0.97	0.98	1.00
			No. 2	R-114	2.01	0	2.01×10^4	63.55	1.37	1.40	1.36	1.54	1.45	1.34	1.39
								129.86	1.07	1.00	0.99	0.98	0.92	0.92	0.99
					2.01	0	2.01×10^4	63.55	1.37	1.40	1.36	1.54	1.45	1.33	1.40
							2.95×10^4		1.01	1.04	1.05	1.06	1.07	1.07	1.05
			No. 3	R-114	2.01	0	2.01×10^4	63.55	1.26	1.23	1.33	1.47	1.39	1.30	1.32
								129.86	0.98	0.97	0.96	0.97	0.97	0.96	0.97
					2.01	0	2.01×10^4	63.55	1.26	1.24	1.33	1.46	1.40	1.29	1.32
							2.95×10^4		1.12	1.14	1.11	1.12	1.15	1.17	1.14
Reid *et al.* [18]	Helical fin	Cu	No. 2	R-113	3.51	17.5	2.33×10^4	380	0.75	0.60	1.13	1.13	1.1	1.15	0.95
			No. 3	R-113	3.44	17.3	2.47×10^4	409	0.61	0.40	0.56	0.55	0.55	0.57	0.55
			No. 5	R-113	3.45	17.8	1.43×10^4	151	2.1	1.42	1.41	1.29	1.05	1.45	1.45
			No. 6	R-113	3.51	19.2	1.43×10^4	154	1.15	0.76	1.06	1.40	1.31	1.4	1.31
			No. 7	R-113	3.44	17.4	1.41×10^4	161	1.16	0.51	0.91	0.95	0.98	1.00	1.00
	Twisted tape	SS	No. 8	R-113	3.46	18.5	1.29×10^4	158	0.73	0.54	0.76	0.71	0.82	0.7	0.69

Underlining indicates the value of enhancement performance ratio less than 1.0.

† Enhancement performance ratio $= ((h_{TP})_{finned}/(h_{TP})_{unfinned})/((\Delta P)_{finned}/(\Delta P)_{unfinned})$.

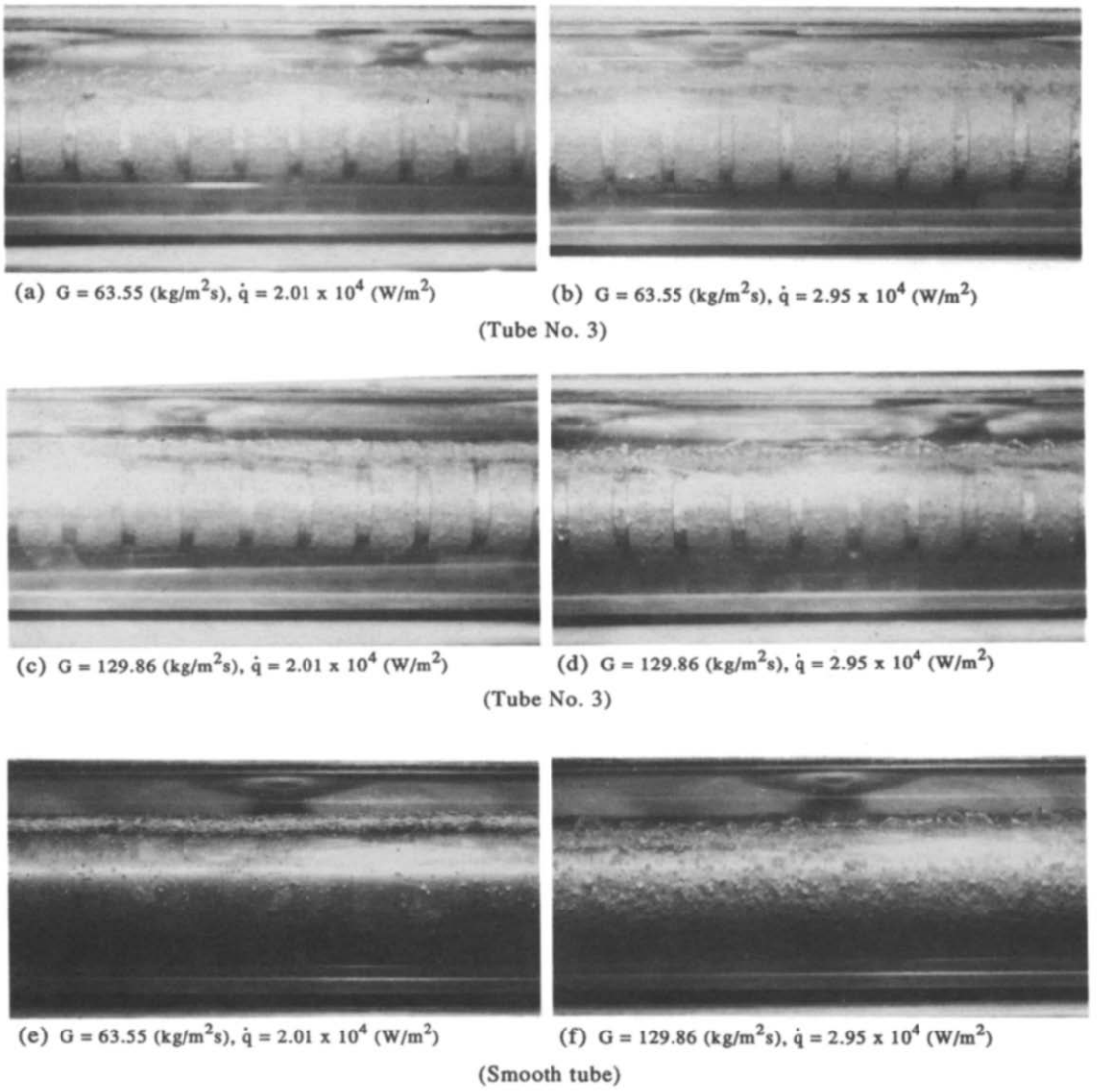

FIG. 13. Photographs made by the flow visualization of nucleate boiling at various mass velocity and heat flux.

CONCLUSION

The present experimental study of evaporation heat transfer in rib roughened tube annuli has made it possible to examine for the first time the effect of a number of parameters. The influence of mass velocity, heat flux, rib geometry to the pressure drop and heat transfer characteristic was examined and discussed. The following conclusions are drawn:

(1) Flow nucleate boiling is enhanced in terms of a lower wall superheat required for incipient boiling and more and stabler bubbles than from a smooth tube.

(2) The present study was in the 'partial nucleate boiling' region. The gradual suppression of the nucleate boiling mechanism results in a reduction of the heat transfer coefficients with increasing quality. However, the transition quality was not found in all the test runs.

(3) The enhancement performance ratios ranged from 0.92–1.54 (see Table 3) depending on the quality, specified mass velocity and heat flux, and the roughened surface geometry.

(4) Because of lower pressure gradient ratio, Tube 2 had a higher enhancement performance ratio (1.54 compared to 0.96 at $X = 0.4$).

(5) Comparisons with those of previous studies roughened by helical fin and twisted tape with R-113 were conducted. The results showed that the enhancement performance ratio of the present study is averagingly higher than those with helical fin and twisted tape for the cases studied herein.

(6) Through flow visualization, the photographs, qualitatively, indicate that the presence of protruding

ribs generates more active and stable nucleation sites and enhances the flow boiling heat transfer.

REFERENCES

1. A. E. Bergles, V. Nirmalan, F. H. Junkhan and R. I. Webb, Bibliography on augmentation of convective and mass transfer—H, Heat Transfer Laboratory Report HFL-31, ISU-ERI-Ames-84221, Iowa State University, Ames, IA (Dec. 1983).
2. J. G. Lavin and E. H. Young, Heat transfer to evaporating refrigerants in two phase flow, *A.I.Ch.E. Jl* **44,** 1424–1432 (1965).
3. G. R. Kubanck and D. L. Miletti, Evaporative heat transfer and pressure drop performance of internally finned tubes with refrigerant 22, *ASME J. Heat Transfer* **101,** 447–452 (1979).
4. M. Ito and H. Kimura, Boiling heat transfer and pressure drop in internal spiral-grooved tubes, *Bull. Jap. Soc. Mech. Engrs* **22**(171), 1251–1257 (1979).
5. H. Kimura and M. Ito, Evaporating heat transfer in horizontal internal spiral-grooved tubes in the region of low flow rates, *Bull. Jap. Soc. Mech. Engs* **24**(195), 1602–1607 (1979).
6. A. Tatsumi, K. Oizumi, M. Hayashi and M. Ito, Application of inner groove tubes to air conditioners, *Hitachi Rev.* **32**(1), 55–60 (1982).
7. K. Tojo, K. Hosokawa, T. Arimoto, H. Yamada and Y. Ohta, Performance characteristics of multigrooved tubes for air conditioners, *Australian Refrigeration Air-Conditioning and Heating* 45–61 (Aug. 1984).
8. T. A. Blatt and R. R. Adt, The twisted tape swirl generators on the heat transfer rate and pressure drop of boiling freon 11 and water, ASME Paper No. 63-WA42 (1963).
9. K. N. Agarwal, H. K. Varma and S. Lal, Boiling of R-12 under swirl flow, *Proceedings Fifth National Heat and Mass Transfer Conference*, Hyderabad, India, pp. 101–106 (Feb. 1980).
10. M. K. Jensen and H. P. Ransler, Saturated forced-convective boiling heat transfer with twisted-tape inserts, *ASME J. Heat Transfer* **107,** 43–47 (1985).
11. R. K. Young and R. L. Hummel, Improved nucleate boiling heat transfer, *Chem. Engng Prog.* **60,** 53–58 (1964).
12. L. Franc, J. B. Brochner, H. P. Domenjond and R. Morin, Improvements made to the thermal transfer of fuel elements by using vapotron process, *Paper A/CONF 28/p/96 Presented at 3rd International Conference on Peaceful Uses of Atomic Energy*.
13. F. W. Dittus and L. M. K. Bolelter, Heat transfer in automobile radiators of the tubular type, University of California Publication in Engng, Vol. 2, No. 13, pp. 443–450. University of California Press, Berkekey (1930).
14. M. M. Shah, Chart correlation for saturated boiling heat transfer: equations and further study, *ASHRAE Trans.* **88,** 185–196 (1982).
15. R. W. Lockhart and R. C. Martinelli, Proposed correlation of data for isothermal two-phase two-component flow in pipes, *Chem. Engng Prog.* **45,** 39–48 (1949).
16. H. Ross, R. Radermacher, M. di Marzo and D. Didion, Horizontal flow boiling of pure and mixed refrigerants, *Int. J. Heat Mass Transfer* **30,** 979–992 (1987).
17. L. W. Reidy, Flat plate drag reduction in a wake tunnel using riblets, Naval Ocean Systems' Center, Technical Report H69 (May 1987).
18. R. S. Reid, M. B. Pate and A. E. Bergles, A comparison of augmentation techniques during in-tube evaporation of R-113, *ASME J. Heat Transfer* **113,** 451–458 (1991).